IOPscience iopscience.iop.org

Home Search Collections Journals About Contact us My IOPscience

A model study of the extended fine structure in the secondary-electron spectra of solids

This article has been downloaded from IOPscience. Please scroll down to see the full text article.

1995 J. Phys.: Condens. Matter 7 5713

(http://iopscience.iop.org/0953-8984/7/28/023)

View the table of contents for this issue, or go to the journal homepage for more

Download details:
IP Address: 171.66.16.151
The article was downloaded on 12/05/2010 at 21:43

Please note that terms and conditions apply.

J. Phys.: Condens. Matter 7 (1995) 5713–5727. Printed in the UK

A model study of the extended fine structure in the secondary-electron spectra of solids

V I Grebennikov and O B Sokolov

Institute of Metal Physics, Russian Academy of Sciences and Udmurt State University, 620219 Ekaterinburg GSP-170, Russia

Received 26 October 1994, in final form 30 March 1995

Abstract. A theory describing the extended oscillations in secondary-electron (SE) spectra and their connections with the short-range atomic structure in solids is developed. We investigate the two main mechanisms for the occurrence of SEs: direct knocking out of SEs from the core level by primary electrons, and a second-order process, called autoionization, going through excitation of a core-level electron into some intermediate states followed by emission of the final SEs. Interference of a direct wave and waves reflected from neighbouring atoms are considered both in the final and in the intermediate states. We derive the cross sections for SEs created in single crystals and polycrystals. In the latter case the signal is described by the two EXAFS-like oscillating functions which are controlled by the final and intermediate energies. The intermediate wave diffraction is described by the EXAFS-like backscattering in all cases. The extended fine structure is expressed, in an explicit form, in terms of coordinates and the scattering characteristics of neighbouring atoms, which opens up new possibilities for obtaining information on the short-range atomic structure near surfaces.

1. Introduction

Recently it has been experimentally observed that CVV Auger lines (transitions involved a core-level hole and two valence electrons) are accompanied by intensity oscillations of secondary electrons (SEs) escaping from solids whose kinetic energies exceed the Auger line energy at 5–500 eV (De Crescenzi *et al* 1986, Chiarello *et al* 1987). By analogy with the extended x-ray absorption fine structure (EXAFS) some workers call this phenomenon the extended Auger fine structure (FS) (De Crescenzi *et al* 1989). At the same time, however, there is an alternative approach (Woodruff 1987) according to which the Auger process is not important for the phenomenon at all, but oscillations arise from a simple electron diffraction of SEs emitted from a point source, just as in the well known photoelectron diffraction in solids (Sinkovic *et al* 1991). Incidentally it should be mentioned that attempts to handle the signals using all the known EXAFS-like formulae have failed (Agostino *et al* 1992).

There has been one quantitative description of the first-order mechanism by Aebi *et al* (1992) based on applying the Fermi golden rule and summing over transitions to all possible scattering states of a given energy. They obtained a strong correspondence between some theoretical and experimental features in Cu in the SE energy interval 150–250 eV, but the theoretical features possess energy-dependent shifts at higher energies than do the corresponding experimental features. Furthermore, their calculations do not reproduce the last three experimental peaks at all.

There is another outstanding question that remains to be answered. Why does the FS have clearly defined Auger lines above (from the higher-kinetic-energy side) and is heavily

0953-8984/95/285713+15$19.50 © 1995 IOP Publishing Ltd

attenuated from the low-energy side? This suggests that the FS includes the formation through the second-order process of virtual excitations of core-level electrons, because the process has an energy threshold at the CVV Auger line, while the first-order process acts at any energies. Moreover, according to the first-order approach the FS is obtained in all types of material where electron scattering on neighbouring atoms has distinct values. However, the FS was experimentally discovered in transition metals (Cu, Ni, Co and Ag) and is absent, for example, in Si (De Crescenzi *et al* 1989). This also suggests the use, in combination with the first-order mechanism, of the autoionization mechanism the contribution of which is proportional to the squared number of core-level electrons and the number of valence electrons (per atom). By this means, the difference between the first and second mechanisms is not only quantitative but also qualitative. That is the reason why we would like to study both types of process in a unified approach. Also, we want to gain a common picture of the phenomenon, i.e. simple equations which give the dependences of the SE FS spectra versus SE energies, the core-level energies of electrons involved in transitions and their numbers. Because of this, the basis for our consideration is the simplest model that, we hope, is capable of describing the main features of the FS formation. We consider the model approach as a necessary first step that has to come before the more realistic numerical calculations taking into account the fine peculiarities of concrete materials.

Therefore, there are problems in elucidating the main mechanisms forming the FS in SE spectra, in developing a theory on the qualitative and quantitative FS description and, finally, in devising a method for retrieval of information on the short-range atomic structures near surfaces. Our goal is to give a solution, in the first approximation, on the basis of the simplest model.

First, we investigate various intrinsic processes of SE creation on a separate atom as a result of inelastic primary-electron scattering. They are the first-order process of directly knocking SEs out of an atom, and the second-order process which will be called autoionization. The main results needed for one atom are given in the next section. Then we consider interference effects for a direct SE wave and waves reflected from neighbouring atoms. In section 3 the FS is investigated as a result of SE diffraction in final states. We obtain a new equation for the angle-integrated SE spectra; it is of EXAFS-like type. In section 4 an autoionization creation of SEs is considered. Special attention is focused on interference effects in intermediate states. This gives an EXAFS-like contribution in all cases. In section 5 the cross sections for various mechanisms are given. In section 6 we discuss the main results concerned with the origin and mathematical description of the extended FS in SE spectra. Estimates of some integrals are given in the appendix.

Core-level ionization and the corresponding autoionization processes are thought to be the major contributors to FS at kinetic energies of 100–500 eV and even at about 1000 eV. However, it is well known that most SEs in solids arise from the process of electron energy losses due to plasmon excitation and single-particle valence excitations which is repeated many times. The energy loss value is about $\Delta E = 5$–30 eV in every separate scattering event. A cascade of such losses gives a more or less homogeneous SE background which can far exceed the intensity of CVV Auger lines, for example. Here we are interested not in the background magnitude but in its FS. We should distinguish between

(1) oscillations in the angular distribution of the SEs at any specific energy and
(2) oscillations in their energy distribution in angle-integrated spectra.

In section 5 we show that (2) is not evidence from (1) at all. The different magnitudes of the diffraction effects in distributions (1) and (2) arises from the strong angle anisotropy of inelastic scattering at small energy transfers ΔE. Small-angle scattering is dominated in

any separate event in the cascade. It is large enough for diffraction to appear in the angle distribution and this is obtained experimentally. For diffraction in angle-integrated spectra, backscattering on angles from $\pi/2$ to π is needed. Its probability is very small for the cascade background mechanism; therefore it does not give a marked contribution in the FS of angle-integrated spectra. By contrast, the mechanisms of SE creation due to core-level electron ionization, considered in this paper, provide scattering on large angles and, because of this, determine the FS in SE spectra.

There is sound experimental evidence to show that the autoionization channel is important. Analysing the SE spectrum of silver metal (De Crescenzi *et al* 1989) we can see that the FS, obtained from the higher-energy side of the $N_{2,3}VV$ Auger line (50 eV), is damped out gradually when the kinetic energy rises. This is natural for any mechanism, but after the $M_{4,5}VV$ line (350 eV) a new FS appears. The two FSs are exhibited also in nickel above the $M_{2,3}VV$ (60 eV) and $L_{2,3}VV$ (920 eV) Auger lines (Guy *et al* 1994). It is quite reasonable that a new autoionization channel opens when the energy reaches the core-level excitation threshold, but we do not see any way in which primary electrons, losing their energy by small portions $\Delta E = 5$–30 eV, can produce two or more signals in different energy regions. Because of this we concentrate on the study of core electron ionization and excitation and consider the background less.

2. The single-atom process

Consider the inelastic scattering of a primary electron with wavevector w on a single atom. The electron transfers into a state of wavevector u, creating a SE of wavevector p due to the transition of an electron from a core level α. The schematic diagram of the states is shown in figure 1(a); it is thought that $p \ll u, w$. The corresponding scattering diagram is displayed on figure 1(b). For a while, we exclude the broken line which denotes scattering on neighbouring atoms; this will be needed in other sections.

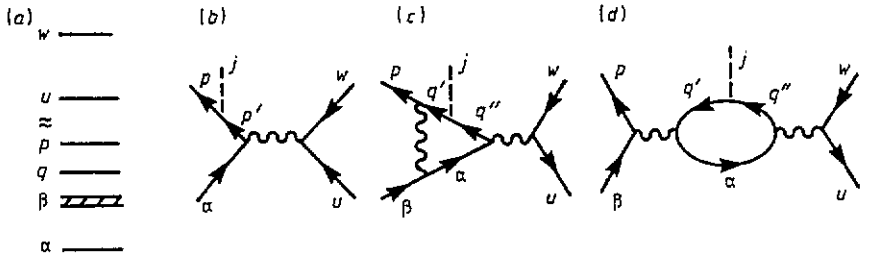

Figure 1. Schematic diagram of energy levels and diagrams for scattering amplitudes.

We have shown (Grebennikov and Sokolov 1994) that, besides the direct knocking out of SEs (due to the first-order Coulomb interaction denoted by a wavy line), the second-order autoionization process plays an important role. Associated direct and exchange diagrams are shown in figure 1(c) and (d). (Once again one can ignore the broken lines.) An electron from a core level α is excited into intermediate states of wavevector q'; then the hole α appearing is annihilated by a valence band electron β with simultaneous q' electron transition into a final state of wavevector p to be measured ($q' \to p$ and $\beta \to \alpha$). The exchange process is given by the transitions $q' \to \alpha$ and $\beta \to p$.

The energy and angle distributions of p electrons have been obtained by Grebennikov and Sokolov (1994). Besides the processes mentioned above, the SEs escape from valence states and their interference with the autoionization channel have also been taken into account. It turns out that their contributions are small in the energy interval to be considered. Recall that our region is situated above the $\alpha\beta\beta$ Auger line, i.e. the kinetic energy $E_p = p^2/2$ exceeds the bond energy $E_\alpha = \alpha^2/2$. For definition purposes, the $M_{2,3}$ level in copper has an energy $E_\alpha = 60$ eV. Another possibility is the $L_{2,3}$ level with energy $E_\alpha = 920$ eV. Everywhere it is thought that $w, u \gg p \simeq \alpha$ and $\beta \ll p, \alpha$.

We believe that the principal results must be obtained in simple models. Therefore we take plane waves (normalized on the δ-function) for the continuum states w, u, p and q, and $|\alpha) = (\alpha^3/\pi)^{1/2}\exp(-\alpha r)$ for the core-level state. The analogous type $|\beta) = N_\beta^{-1/2}\exp(-\beta r)$ is taken for the valence band wavefunction (the wavevector is omitted because of its smallness compared with p). Under these assumptions we have obtained the following results (atomic units are used).

The first-order cross section for SEs with a wavevector p takes the form

$$\frac{d^2\sigma_\alpha(p)}{dE\,d\Omega} = 2n_\alpha\sigma_0(|T^0(p)|^2)_{\hat{u}} \qquad \sigma_0 = \frac{64\pi^5 a_0^2 pu}{w} \tag{1}$$

where the amplitude is

$$T^0(p) = \frac{(2\alpha^5)^{1/2}}{\pi^3\kappa^2(\alpha^2 + |p-\kappa|^2)^2} \qquad \kappa = w - u \qquad u^2 = w^2 - p^2 - \alpha^2. \tag{2}$$

Here a_0 is the Bohr radius and $2n_\alpha$ is the number of electrons on the level α (n_α is the number of orbitals and the factor 2 arises from the spin states). The symbol $\hat{}$ denotes the direction of the corresponding vector and the angular brackets denote averaging over the directions (in the given case, over the directions of the scattered electron of wavevector u). At $p \simeq \alpha$ the angle anisotropy is not large. After integrating (1) over all angles $d\Omega$, we obtain the spectral distribution

$$\frac{d\sigma_\alpha/a_0^2}{dE_p/\mathrm{Ryd}} = \frac{16n_\alpha p}{\alpha^7}\left(\frac{2}{1 + p^2/\alpha^2}\right)^6 k \qquad p^2 = \frac{E_p}{\mathrm{Ryd}} \tag{3}$$

where k is a slowly varying function of order 1.

The integral intensity of the spectrum (3) gives the ionization cross section for the level α:

$$\sigma_\alpha \simeq 2n_\alpha\pi a_0^2/(E_\alpha/\mathrm{Ryd})^2. \tag{4}$$

The second-order amplitude (figures 1(*c*) plus 1(*d*)) is equal to

$$D^0(p) = \int d^3q'\, M(p, q')\frac{2n_\alpha}{q^2 - q'^2 + 2i\eta}T^0(q') \tag{5}$$

where

$$M(p, q) = (\pi^3 N_\beta)^{-1/2}\left(\frac{1}{|p-q|^2} - \frac{2}{p^2}\right)\frac{4\alpha^{5/2}}{(\alpha^2 + |p-q|^2)^2}. \tag{6}$$

Here $2E_q = q^2 = p^2 - \alpha^2 = w^2 - u^2 - \alpha^2$ The auxiliary energy E_q corresponds to the rigid conservation law in the intermediate states (we set the valence electron energy $E_\beta \simeq 0$). Recall that the intermediate-state energies $E_{q'}$ need not be equal to E_q.

Making an approximate estimate of the integral in (5), we write the autoionization cross section as follows:

$$\frac{d\sigma_2/a_0^2}{dE_p/\mathrm{Ryd}} = C\left(1-\frac{\alpha^2}{p^2}\right)\frac{16n_\alpha p}{\alpha^7}\left(\frac{2}{p^2/\alpha^2}\right)^6 k \tag{7}$$

where

$$C = \frac{16n_\alpha n_\beta}{E_\alpha/\mathrm{Ryd}}\left(\frac{E_\beta}{E_\alpha}\right)^{3/2}. \tag{8}$$

For the $M_{2,3}$ level in copper, $E_\alpha = 60$ eV and $n_\alpha = 3$, the average energy and the number of valence states are $E_\beta = 5$ eV and $n_\beta = 5$, which gives $C \simeq 1$; therefore the autoionization contribution exceeds that from the first-order process, (figure 2). Recall that the curves in actuality present small additions to the background arising from the inelastic losses of primary electrons. For the $L_{2,3}$ level, $E_\alpha = 920$ eV; it follows that $C \simeq 0$, and the weight of autoionization is negligible. So, the value of the coefficient C (8) characterizes the relative contribution of autoionization to the SE spectra.

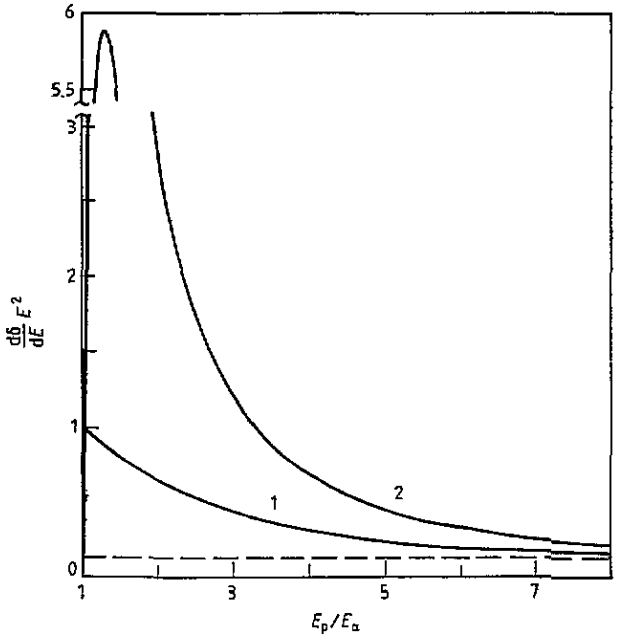

Figure 2. Atomic cross sections in the model for the $M_{2,3}$ level in copper (arbitrary units): curve 1, the first-order process; curve 2, the second-order process; – – –, the valence electron contribution.

The ratio of the full cross section of the second-order process to the α level ionization cross section σ_α is

$$\sigma_2/\sigma_\alpha = 0.47C. \tag{9}$$

Recall that σ_α is equal to a sum of the Auger and autoionization cross sections (we neglect the small contribution of the x-ray decay of the core hole). In particular, it follows that the integral intensities of autoionization and the Auger line in the case of the $M_{2,3}$ level in copper are almost equal to each other.

Of course, we used a very crude model for real metals, but, it seems to us, that the main conclusion about the importance of the second-order process still holds for more realistic approaches, as well. Similar estimations based on 3p wavefunctions reduce the relative weight of the autoionization channel. Nevertheless, the ratio of the second-order to the first-order contributions is controlled by the factor C (8), as before.

It should be remembered that the C-value is proportional to the number of core-level orbitals and to the number of valence electrons per atom. This makes the autoionization contribution higher in transition metals with filled or almost filled d bands.

To avoid confusion, note that the single-atom cross sections σ_1 and σ_2 are among the factors that affect the FS. Also the FS is determined by the corresponding structure factors (see section 5).

3. Secondary electron diffraction

In this section the diffraction effects after SE creation on angle-resolved and angle-integrated spectra are discussed.

3.1. Single scattering on neighbouring atoms

Now we take into account SE elastic scattering on a neighbouring atom. This is shown by broken lines in figure 1. Consider the first-order amplitude b. Take the position of the atom, where the SE is created, as the origin of the coordinates. The process of SE creation on the central atom itself is described by the amplitude $T^0(r)$; its Fourier transform $T^0(p)$ is given in equation (2) for our simple model. The propagation of waves from a point r_1 to a point r_2 is described by the Green function (GF) $G(r_2, r_1)$; then elastic scattering on the potential $W_j(r - R_j)$ of the atom with number j centred at R_j occurs, and the SE reaches its final state $|p) = \phi_0(r_2)$. As a result, the amplitude of the complete process is written as the coordinate integral

$$T_j(p) = \int \phi_p^*(r_2) W_j(r_2 - R_j) G(r_2 - r_1) T^0(r_1). \tag{10}$$

The free GF has the standard form

$$G(r_2, r_1; p) = \int \frac{d^3q}{(2\pi)^3} \frac{\exp[iq \cdot (r_1 - r_2)]}{E_p - E_q + i\eta} = -\frac{\exp(ip + |r_2 - r_1|)}{2\pi |r_2 - r_1|} \tag{11}$$

where

$$p^+ = p + i\gamma \qquad p^{+2}/2 = E_p + i\eta.$$

The coordinate $r_1 = \rho_1$ in (10) is restricted in the range of the core wavefunctions α and the second coordinate $r_2 = R_j + \rho$ is localized near the neighbouring atom R_j due to the short-range character of the potential W_j. This gives an opportunity to use the standard expansion $|R_j + \rho_2 - \rho_1| \simeq R_j + e_j \cdot (\rho_2 - \rho_1)$, where $e_j = R_j/R_j$ is a unit vector along

a neighbouring atom direction, and we arrive at the well known plane-wave approximation (PWA) for the GF:

$$G(R_j + \rho_2, \rho_1) = (-2\pi R_j)^{-1} \exp(ip^+ R_j) \exp[i\boldsymbol{p}_j \cdot (\rho_2 - \rho_1)] \tag{12}$$

where, by definition, $\boldsymbol{p}_j = p\boldsymbol{e}_j$ is the wavevector along direction $\boldsymbol{e}_j$. The imaginary addition $i\eta$ characterizes the finite width of excited states in many-body systems. It generates an imaginary addition $i\gamma$ in the wavevector $p^+ = p + i\gamma$, which describes the electron wave damping in space in (11). Assuming that the final state $\phi_p(r)$ is the normalized plane wave, we obtain

$$T_j(\boldsymbol{p}) = f_j(p, \theta_j) R_j^{-1} \exp(ip^+ L_j) T^0(\boldsymbol{p}_j) \tag{13}$$

where the Fourier transform of the scattering potential given by

$$W_j(\boldsymbol{p}, \boldsymbol{p}_j) = \int d^3\rho \, W_j(\rho) \exp[i(\boldsymbol{p}_j - \boldsymbol{p}) \cdot \rho] \to -2\pi f_j(p, \theta_j) \tag{14}$$

is changed to the amplitude $f_j(p, \theta_j)$ of plane-wave elastic scattering on an angle θ_j between the incident $\boldsymbol{p}_j$ and scattered $\boldsymbol{p}$ waves. This correction is accounted for by multiple scattering on the potential W_j. The length $L_j = R_j(1 - \cos\theta_j)$ is the path difference for the wave scattered on site j and the direct wave. Of course, multiple scattering of the SEs on the central atom also changes the source function $T^0(\boldsymbol{p})$ (2) approximately, together with (14), but this is a quantitative correction only.

So all details of the origin of SEs and their scattering on the centre atom are contained in the function $T^0(\boldsymbol{p})$, and elastic scattering on the neighbouring atom is described by the value $f_j(p, \theta)$. The latter takes into account the spherical character of the scattered waves (Sinkovic *et al* 1991) if we introduce the dependence on the distance R_j. The phase factor, in the middle of equation (13), is responsible for the structure in the diffraction picture.

The equation of type (13) is well known, and it is widely used for the description of photoelectron diffraction in solids (Sinkovic *et al* 1991). Below we shall derive a new simple angle-integrated equation for electron diffraction.

3.2. Scattering on atom pairs

Of all kinds of atom pair, scattering on a site j accompanied by scattering on the centre O stands out, because in this case the path differences for all waves reflected from atoms, possessed by the same coordination sphere, are equal. The corresponding matrix elements have the structure $T_{0j}(\boldsymbol{p}) = \phi_p W_0 G_{0j} W_j G_{j0} T^0$. Using the PWA (12) for intersite GFs and replacing the Fourier transforms of potentials on their scattering amplitudes (14), we come to the equation

$$T_{0j}(\boldsymbol{p}) = ip\chi_j(p) f_0(p, \pi - \theta_j) T^0(\boldsymbol{p}_j). \tag{15}$$

Here we introduce the function

$$\chi_j(p) = (ipR_j^2)^{-1} \exp(2ip^+ R_j) f_j(p, \pi) \tag{16}$$

describing backscattering on an atom j. It looks very much like the well known EXAFS function (Sayers *et al* 1970).

3.3. The average amplitude

Owing to the weakness of elastic scattering T_j compared with T^0, the SE spectra in polycrystals are determined by the amplitude $\langle T_j(\boldsymbol{p})\rangle_{e_j}$ (13), averaged over all possible orientations e_j of neighbouring atoms. To estimate this, we direct the z axis of the spherical coordinate system along the vector $\boldsymbol{p}$; then the angle-averaged function (13) becomes

$$\langle T_j\rangle = \frac{1}{4\pi}\int_0^{\pi} \mathrm{d}\theta\, \sin\theta \exp(-\mathrm{i}pR\cos\theta)\int_0^{2\pi}\mathrm{d}\phi\, F(\theta,\phi)$$

$$= \frac{1}{2\mathrm{i}pR}[\exp(\mathrm{i}pR)F(\pi) - \exp(-\mathrm{i}pR)F(0)] - \frac{1}{4\pi}\int\cdots. \tag{17}$$

Here the angle-dependent phase factor $\exp(-\mathrm{i}pR\cos\theta)$ is evolved explicitly from the function T_j and the rest function is denoted as F. Then the integral over θ is taken by parts, and the new integral term appearing is only symbolized. As a result of exponent integration, the factor $(pR)^{-1} \ll 1$ arises. If the symbolized integral in (17) is small compared with the first term, we obtain the estimation

$$\langle T_j(\boldsymbol{p})\rangle_{e_j} \simeq [\chi_j(p)T^0(-\boldsymbol{p}) - C_j(p)T^0(\boldsymbol{p})]/2 \tag{18}$$

where $C_j(p) = (\mathrm{i}pR_j^2)^{-1} f_j(p,0)$. As is shown in the appendix, the estimation (18) holds true for the fully consistent consideration but, in this case, the contribution C_j from forward scattering should be scaled down. For the screened Coulomb potential with radius r_0,

$$C_j(p) = 2R_j^{-1} f_j(p,\pi)[0.577 - \ln(2pr_0^2/R) - \mathrm{i}\pi/2]. \tag{19}$$

Hence, averaging over orientations of neighbouring atoms in polycrystals, amorphous matter, etc, provides the oscillating EXAFS-like function $\chi(p)$ and some additional background $C(p)$ for ordinary electron diffraction. In our view, this is a new and useful result for traditional SE diffraction theory.

4. Diffraction in autoionization

Elastic scattering on neighbouring atoms modifies the intra-atomic autoionization process described in section 2 in two ways: firstly because of electron scattering after SE creation; secondly because of scattering in intermediate states during autoionization itself.

4.1. Scattering after autoionization

This is described by figures 1(*c*) and 1(*d*) except that the broken line is not in the middle of the diagram as shown in the figures, but at line p, as in figure 1(*b*). For this case the final results are similar to those of section 3, where the matrix element $T^0(\boldsymbol{p}_j)$, describing the SE creation in the state of wavevector $\boldsymbol{p}_j$ should be replaced by the corresponding second-order autoionization element $D^0(\boldsymbol{p}_j)$ (5). So, the amplitude D_j of autoionization accompanied by following elastic scattering on a neighbouring atom is given by an equation of type (13):

$$D_j(\boldsymbol{p}) = f_j(p,\theta_j)R_j^{-1}\exp(\mathrm{i}p^+L_j)D^0(\boldsymbol{p}_j). \tag{20}$$

However, producing equation (20) is more complicated than equation (13) by virtue of the fact that $T^0(\boldsymbol{r})$ is localized at the atom at the origin but the corresponding function $D^0(\boldsymbol{r})$ is only centred on that atom and can spread far from it owing to the rather small attenuation

of the Coulomb interaction. As a result, the validity of the PWA for the GF connected with a source of scatter j in an equation such as (10) is not evident.

To obtain (20) we start from the exact expression

$$D_j(\boldsymbol{p}) = \int \frac{\mathrm{d}^3 p'}{(2\pi)^2} f_j(\boldsymbol{p}, \boldsymbol{p}') \frac{2\exp[\mathrm{i}(\boldsymbol{p}' - \boldsymbol{p}) \cdot \boldsymbol{R}_j]}{p'^2 - p^{+2}} D^0(\boldsymbol{p}')$$

and integrate it over angle variables by parts in the sense of (17). Then we arrive at integrals of the type $J_\pm$ (A5) from the appendix and their estimations furnish the result (20).

The average amplitude of polycrystals (amorphous matter or angle-integrated experiments) is identical with (17):

$$\langle D_j(\boldsymbol{p}) \rangle_{e_j} \simeq [\chi_j(p) D^0(-\boldsymbol{p}) - C_j(p) D^0(\boldsymbol{p})]/2. \tag{21}$$

4.2. Scattering in intermediate states

This is described by figures 1(c) and 1(d), where elastic scattering on neighbouring atoms takes place between primary excitation and emission of final electrons or, which is the same, the intermediate-state perturbation due to other atom potentials is taken into account. A corresponding amplitude is formed of type $S_j = MGf_jG_{j0}T^0$. If we make allowance for (10), (11) and (13), this becomes

$$S_j(\boldsymbol{p}) = \int \mathrm{d}^3 q'\, M(\boldsymbol{p}, \boldsymbol{q}') \frac{2n_\alpha}{q^{+2} - q'^2} T_j(\boldsymbol{q}'; \boldsymbol{q}) \tag{22}$$

where

$$T_j(\boldsymbol{q}'; \boldsymbol{q}) = f_j(\boldsymbol{q}', \boldsymbol{q}_j) R_j^{-1} \exp[\mathrm{i}(q^+ - q' \cos\theta_j) R_j] T^0(\boldsymbol{q}_j) \tag{23}$$

$f_j(\boldsymbol{q}', \boldsymbol{q}_j)$ is the amplitude of plane-wave scattering from $\boldsymbol{q} = q\boldsymbol{e}_j$ state into the $\boldsymbol{q}'$ state on the potential W_j. At $q' = q_j$, equation (23) turns into equation (13).

It is very simple to take the integral in (22) for the bubble (exchange) diagram in figure 1(d) because the electron of wavevector $\boldsymbol{q}'$ transfers into a short-range inner state α, which gives us the opportunity to use the PWA for the GF in (22).

In the direct diagram, figure 1(c), the electron goes from one delocalized $\boldsymbol{q}'$ state into another delocalized $\boldsymbol{p}$ state, and connection with the central atom is controlled only by the long-range Coulomb interaction. Nevertheless, a contribution from elastic backscattering prevails in this case, too. To show this, we rewrite the denominator in the integral (22) in the form of two fractions $2q'/(q^2 - q'^2) = 1/(q - q') - 1/(q + q')$. After changing variables $q' \to -q'$ in the second item and reversing the direction $\hat{q}' \to -\hat{q}'$ to conserve the rest under the integral functions, we obtain

$$S_j(\boldsymbol{p}) = 4\pi \int_{-\infty}^{\infty} \frac{q'\,\mathrm{d}q'}{q^+ - q'} \langle M(\boldsymbol{p}, \boldsymbol{q}') T_j(\boldsymbol{q}'; \boldsymbol{q}) \rangle_{q'}. \tag{24}$$

Using an estimation of type (17), this leads to the equation

$$S_j \simeq \frac{2\pi}{\mathrm{i}R^2} \int \frac{\mathrm{d}q'}{q^+ - q'} [M(\boldsymbol{p}, \boldsymbol{q}'_j) f(-\boldsymbol{q}'_j, \boldsymbol{q}_j) \exp(\mathrm{i}q'R) - M(\boldsymbol{p}, \boldsymbol{q}'_j) f(\boldsymbol{q}'_j, \boldsymbol{q}_j) \exp(-\mathrm{i}q'R)]$$
$$\times \exp(\mathrm{i}qR) T^0(\boldsymbol{q}_j).$$

Evaluating integrals by equation (A5) from the appendix we find the final result

$$S_j(p) = -4\pi^2 \mathrm{i} q \chi_j(q) M(p, -q_j) T^0(q_j). \tag{25}$$

Note that there is a correspondence between scattering S_j (25) and backscattering T_{0j} (15) under the condition $-4\pi^2 M(p, -q) \to f_0(p, \pi - \theta)$. However, the oscillations in (25) are controlled not by the final but by the intermediate energy $q^2 = p^2 - \alpha^2$.

In conclusion, the intermediate-state perturbation due to the neighbouring atoms leads to the EXAFS-like oscillations $\chi(q)$ in the autoionization channel even in single crystals. This is the specific peculiarity of the second-order process.

The amplitude in polycrystals is obtained by averaging (25) over all q_j directions. This can be represented by

$$\langle S_j(p) \rangle_{e_j} = \mathrm{i}\chi_j(q) \int \mathrm{d}^3 q_j \, M(-p, q_j) \operatorname{Im}\left(\frac{2}{q^{+2} - q_j^2}\right) T^0(q_j) = \mathrm{i}\chi(q) \operatorname{Im}[D^0(-p)]. \tag{26}$$

The last equation is written on the assumption that functions M and T^0 may be chosen to be real, for example as in (2) and (6).

5. The SE spectra

By spectrum we mean the current created by the SE with a definite energy and p direction. Another characteristic of the process is given by its cross section

$$\frac{\mathrm{d}^2\sigma(p)}{\mathrm{d}E \, \mathrm{d}\Omega} = \sigma_0 \langle |\mathbf{T}(p; u)|^2 \rangle_{\hat{u}}. \tag{27}$$

Here $\mathbf{T}$ denotes the full matrix of the transition of the primary electron of wavevector w into the u state on ejecting the SEs in the p state with energy $E = p^2/2$ in the space angles $\mathrm{d}\Omega$. It can be shown that there is a simple connection

$$\exp(-2\gamma r) \, \mathrm{d}\sigma(p)/\mathrm{d}E = \mathrm{d}I_p/|j_W| \tag{28}$$

between the cross section in the p direction and the current $\mathrm{d}I_p = j_p r^2 \, \mathrm{d}\Omega$ normalized with respect to the density j_w of the primary beam current. It is the damping on the left-hand side of (28) that requires us to introduce the damping $\exp(-\gamma r)$ in the wavefunction and the corresponding imaginary addition $p^+ = p + \mathrm{i}\gamma$ in equation (13), etc, together with the total path difference L_j of interference waves.

The first-order cross section is determined by the amplitude $T_1 = T^0 + T_j + T_{0j}$, which is the sum of the atomic (single-centre) amplitude T^0 (2), the small corrections T_j (13) for scattering on neighbouring atoms and the subsequent additional scattering T_{0j} (15) on the centre. The subscript 1 indicates that the final state is formed by single inelastic scattering. As a result, a hole is present in the core level α in final states.

Another group of final states arise in autoionization, namely the double inelastic process. In this case the core level is occupied and the hole elevated to the valence band. Summing (5), (20) and (25), and also the pair scattering analogue of (15), D_{0j}, we obtain $T_2 = D^0 + D_j + D_{0j} + S_j$.

The main contributions in T_1 and T_2 arise from the first terms T^0 and D^0. The relation between these have been described in section 2 (see also Grebennikov and Sokolov (1994)). The rest leads to the FS.

5.1. The first-order cross section

Substituting T_1 into (27), we find in the linear approximation that

$$\frac{d^2\sigma_1(p)}{dE\,d\Omega} = 2n_\alpha\sigma_0\Big[\langle|T^0(p)|^2\rangle_{\hat{u}} + 2\,\mathrm{Re}\Big(\sum_j \langle T^{*0}(p)T^0(p_j)\rangle_{\hat{u}}[f_j(p,\theta_j)R_j^{-1}\exp(ip^+L_j) + f_0(p,\pi-\theta_j)ip\chi_j(p)]\Big)\Big]. \tag{29}$$

In the polycrystalline case the cross section is determined by equation (29) averaged over different atom directions:

$$\left\langle\frac{d\sigma_1(p)}{dE\,d\Omega}\right\rangle_{e_j} = 2n_\alpha\sigma_0\langle|T^0(p)|^2\rangle_{\hat{u}}\Big[1 + \mathrm{Re}\Big(\sum_j[\mu\tilde{\chi}_j(p) - C_j(p)]\Big)\Big] \tag{30}$$

where

$$\tilde{\chi}_j(p) = \chi_j(p)[1 + 2ip\langle f_0(p,\theta_j)\rangle_{e_j}] \tag{31}$$

is the function (16) renormalized owing to $0j$ pair elastic scattering, and $\mu = \langle T^{*0}(p)T^0(-p)\rangle_{\hat{u}}/\langle|T^0(p)|^2\rangle_{\hat{u}}$ is a coefficient equal to about 1 at $p \simeq \alpha \ll w$, i.e. in the case when anisotropy of the single-atom cross section is small.

The signal (30) is described by the product of the single-atom cross section on the oscillating function $\chi(p)$. Also scattering on atoms generates the additional background $C(p)$.

The first term in (29) and (30) describes the single-atom cross section. Neighbouring-atom effects are given by two factors: atomic and structural. The atomic factor (correlator) $\langle T(p)T(p_j)\rangle \equiv I(p,\theta_j)$ is defined as the averaged product of creation amplitudes for two waves. The first propagates in the selected p direction and the other goes to a neighbouring atom j. In fact, $I(p,\theta_j)$ determines the intensity of the source of the waves. The structural factor describes interference between the waves after scattering one of them on a neighbouring atom j.

The angle-averaged equation (30) is controlled by two extreme angles $\theta = \pi$ and 0. The amplitude of oscillations in angle-integrated spectra is proportional to the correlator $I(p,\pi)$. Its estimations give us an opportunity to select the most important mechanisms for FS formation.

In this connection consider the cascade mechanism that forms the SE background. The initial electron loses its energy many times in small portions most of which are due to plasmon excitations and single-particle valence excitations. The losses ΔE = 5–30 eV are small compared with the energies E = 100–500 eV considered. Under this condition most electrons scatter at small angles. It is easily seen, for example, from equation (2) which has to be used now for electrons of type u (in the notation of figure 1). It is also necessary to change p to u in (29) and (30). The value α^2 may be considered as the valence electron energy, and $p^2 + \alpha^2 = \Delta E/\mathrm{Ryd} \ll w^2, u^2$. For large angles between u and w the amplitude $T(u) \propto (w-u)^{-6} \simeq (2u\sin\theta/2)^{-6}$. Therefore the back-scattering correlator $I(u,\pi)$ almost disappears. For the space distribution (29), small-angle scattering is quite sufficient and we see that its amplitude $T(u) \propto (u\theta)^{-2}$ is rather large. We believe that the cascade background mechanism yields diffraction effects on the angle distribution but, at the same time, it does not give an essential contribution to FS in the angle-integrated spectra owing to the strong anisotropy of the elementary scattering event.

Electrons knocked from core levels have an almost isotropic distribution at $p \simeq \alpha$. Therefore they can give a larger contribution to the FS in the SE spectra. Even in the $p \gg \alpha$ case, p electrons are emitted at about 90° to the primary electron direction w which also leads to a rather large magnitude of $I(p,\pi)$.

5.2. The second-order cross section

Consider now the second-order cross section $d\sigma_2$, which, as has been discussed, can exceed $d\sigma_1$ in practically important cases.

Substitution of T_2 in (27) results in the autoionization cross section

$$\frac{d^2\sigma_2(p)}{dE\,d\Omega} = 2n_\beta\sigma_0\Bigg[\langle|D^0(p)|^2\rangle_{\hat{u}} + 2\,\mathrm{Re}\Bigg(\sum_j\{\langle D^{*0}(p)D^0(p_j)\rangle_{\hat{u}}[f_j(p,\theta_j)R_j^{-1}\exp(ip^+L_j) + f_0(p,\pi-\theta_j)ip\chi_j(p)] - \langle D^{*0}(p)M(p,-q_j)4\pi^2 iqT^0(q_j)\rangle_{\hat{u}}\tilde{\chi}_j(q)\}\Bigg)\Bigg]. \tag{32}$$

Here the last term is new compared with $d\sigma_1$. It arises from scattering in intermediate states, namely S_j (25) and S_{0j}. The pair scattering S_{0j} of intermediate electrons of the type (15) renormalizes the function $\chi(q)$ as in (31).

In polycrystals (angle-integrated cross section),

$$\left\langle\frac{d^2\sigma_2(p)}{dE\,d\Omega}\right\rangle_{e_j} = 2n_\beta\sigma_0\langle|D^0(p)|^2\rangle_{\hat{u}}\Bigg[1+\mathrm{Re}\Bigg(\sum_j\{\mu_2[\tilde{\chi}_j(p)+2\cos\psi\exp(i\psi)\tilde{\chi}(q)]-C_j(p)\}\Bigg)\Bigg]. \tag{33}$$

The coefficients, determined by the weights of the final p- and intermediate q-state contributions, are given by the equations

$$\cos[\psi(p)] = \mathrm{Im}[D^0(p)/|D^0(p)|]$$

$$\mu_2 = \langle\langle D^{*0}(p)D^0(-p)\rangle\rangle_{\hat{u}}/\langle|D^0(p)|^2\rangle_{\hat{u}}.$$

Note that the EXAFS-like function (31) is included in cross sections in the form

$$\mathrm{Re}[\tilde{\chi}_j(p)] = (pR_j^2)^{-1}|f_j(p,\pi)|\sin(2pR_j+\phi_j+\Delta\phi_0)\exp(-2\gamma R_j) \tag{34}$$

where ϕ_j is the back-scattering phase shift on an atom j, and $\Delta\phi_0$ is the phase shift on the central atom determined from the equation

$$\exp(i\Delta\phi_0) \simeq 1 + 2ip\langle f_0(p,\theta_j\rangle_{e_i}. \tag{35}$$

Considering (32) again, note that the autoionization oscillating signal consists of two contributions. The first arises from the direct- and scattered-wave interference, as in the first-order process (29), but moreover there are EXAFS-like oscillations $\chi(q)$ arising from the intermediate electron q backscattering.

In the polycrystalline case (33), angle averaging leads to two EXAFS-like signals (34) from both final and intermediate states (Grebennikov and Sokolov 1992, Guy *et al* 1993).

6. Discussion

We have considered two main mechanisms responsible for the FS in SE spectra:

(1) direct knocking of SEs from core levels accompanied by interference between a direct wave and a wave scattered on neighbouring atoms, which have been proposed by Woodruff (1987);

(2) the autoionization second-order process put forward by De Crescenzi *et al* (1986, 1989).

We have indicated the probable reason why the SE background contains diffraction effects in the angle distribution at any specific energy and why these effects are highly suppressed in the energy distribution in angle-integrated spectra. The reason is that the small-angle scattering dominates the elementary event of the background cascade owing to small energy losses at plasmon and single-particle valence excitations.

The first-order cross section is written as in equation (29), which is similar to relevant common equations in the theory of photoelectron (Sinkovic *et al* 1991) or Auger electron (Agostino *et al* 1994) diffraction. We have shown that the interference of an electron wave from a point source and a wave scattered on neighbouring atoms leads to EXAFS-like oscillations $\chi(p)$ after averaging over all directions (equation (30)). The oscillations are described by single elastic backscattering. What is more, a monotonic addition to the atomic cross section exists. The result is correct at $pR \gg 1$ for polycrystals, amorphous matter, etc, and also for the angle-integrated SE spectra.

The oscillations arise because the momentum transfer ends at its maximal value $2p$ abruptly. Note that, in experiments on single crystals, integrations are carried out over finite reception angles. This blurs the transfer boundary and can produce some attenuation of signals.

The autoionization process goes through the intermediate excited q states. The FS in single crystals is formed by two mechanisms (32). They are firstly final electron p scattering on definite diffraction angles, just as in the first-order case (29) and secondly intermediate electron backscattering with a wavenumber $q = (p^2 - \alpha^2)^{1/2}$ (the last term in (32)). After angle averaging (polycrystals, etc) the contribution of the p electron becomes EXAFS like too, as was described above for first-order ionization. As a result, the extended FS (33) is controlled by two oscillating functions $\chi(q)$ and $\chi(p)$ (34). The structure factor χ (34) has a strong p dependence. Apart from the multiplier p^{-1}, it contains the backscattering amplitude $f \propto p^{-2}$. Also, the phases $2pR_j$ are very sensitive to the interatomic distance variations at large p. For example, averaging over chaotic thermal (and zero-point) atomic motions gives rise to the Debye–Waller factor $\exp(-2\langle\Delta R_j^2\rangle p^2)$. Since the intermediate-state energy $q^2 = p^2 - \alpha^2$ is smaller than the final-state energy p^2, usually $\chi(q)/\chi(p) > 1$. The ratio becomes particularly high for deeper levels. We expect that the FS above the $L_{2,3}VV$ Auger line in copper ($E = 920$ eV) is controlled by the autoionization mechanism despite the fact that the second-order single-atom cross section is very small: $C = \sigma_2/\sigma_1 \ll 1$; see (8). The experimental FS (Guy *et al* 1994) is obtained in a small energy interval of about 100 eV. This is easy to understand if one takes into account the strong q-dependent structural function $\chi(q)$. In the $M_{2,3}VV$ case, the values of p and q look very similar in the energy region 100–400 eV and, to describe the extended FS, we need to take into account diffraction both in the final and in the intermediate states.

The relation of the extended FS with the coordinates and scattering characteristics of neighbouring atoms opens up new possibilities for determining the short-range atomic structure near the solid surfaces using oscillations in the SE spectra.

Acknowledgments

The research described in this publication was made possible in part by grant RGA000 from the International Science Foundation.

Appendix

Let us calculate the function $T_j(\boldsymbol{p})$ (13) averaged over every possible direction $\boldsymbol{e}_j$. For simplicity, we consider scattering on the screened Coulomb potential with a radius r_0 and an effective charge Z: $W(\rho) = -Z/\rho \exp(-\rho/r_0)$. In the Born approximation for a scattering amplitude (14), after neglecting the angle dependence on $T^0(\boldsymbol{p})$ (which is reasonable for $p^2 \simeq \alpha^2 \ll w^2$), we obtain the equation

$$\langle T(\boldsymbol{p})\rangle_e = \langle \exp[ip^+ R(1-\cos\theta)]2Z/(|\boldsymbol{p}-p\boldsymbol{e}|^2 + r_0^{-2})\rangle_e T^0/R. \tag{A1}$$

We omit the atom number index j hereafter. Since $|\boldsymbol{p}-p\boldsymbol{e}|^2 = 2p^2 y$, where $y = 1-\cos\theta$, averaging in (A1) results in the integral

$$I = \int_0^2 \frac{\mathrm{d}y\, Z \exp(ip\mathrm{Ryd})}{2p^2 y + r_0^{-2}} \tag{A2}$$

which can be transformed into two standard exponential integral functions with an imaginary argument (with allowance for damping $p \to p^+ = p + i\gamma$ with a complex value). First, we determine typical parameter values.

Let the SE energies be $E/\mathrm{Ryd} = p^2 = 9$–36; then the wavevector values $p = 3$–6 au. The nearest-neighbour atom distance in copper is $R \simeq 5$ Bohr radii. Put $r_0 = R/2$, i.e. the potential is screened within the muffin-tin sphere. As a result, we obtain that $pR > 15$ and, therefore $(pR)^{-1}$ is a small perturbation parameter.

Now we rewrite (A2) as a sum of two integrals: $I = \int_\infty^2 + \int_0^\infty$. We integrate the first by parts N times:

$$\int_\infty^2 = \frac{Z}{4p^2 + r_0^{-2}} \frac{\exp(2ipR)}{ipR}\left[1 + \sum_{n=1}^{N+1}\left(\frac{1}{4p^2 + r_0^{-2}}\frac{2p^2}{ipR}\right)^n n!\right]. \tag{A3}$$

The last $N+1$ item was obtained by evaluating the integral by replacement of the pre-exponential function to its maximum value.

After substitution of variables in the second integral, from 0 to ∞, we obtain the standard function

$$\int_0^\infty \frac{Z}{2p^2}\exp(-ix^+)\int_x^\infty \frac{\mathrm{d}t}{t}\exp(it^+)$$
$$= \frac{-Z}{2p^2}\exp(-ix^+)\left(C + \ln x^+ - i\frac{\pi}{2} + \frac{ix^+}{1\times 1!} + \frac{(ix^+)^2}{2\times 2!} + \cdots\right) \tag{A4}$$

where $x = R/2pr_0^2$, $t^+ = tp^+/p$, $x^+ = xp^+/p$ and $C = 0.577\ldots$ is the Euler constant.

Keeping only the leading term ($x \ll 1$), in (A3) and (A4) we obtain (16), (18) and (19).

Now estimate the integrals

$$J_\pm = \int_{-\infty}^{\infty} \frac{\mathrm{d}q'\, f(q')\exp[\pm i(q'-q)R]}{q'-q^+} \qquad R>0 \qquad q^+ \equiv q + i\gamma. \tag{A5}$$

Using the Cauchy-type integral, we introduce the piecewise analytical function from a complex variable z:

$$F(z) = \int_{-\infty}^{\infty} \frac{\mathrm{d}q'\, f(q')}{(q'-z)} \qquad f(q) = \frac{F^+(q) - F^-(q)}{2\pi i} \tag{A6}$$

where $F^{\pm}(q) = F(z = q \pm i0)$ are the limiting values of the function (A6) on the real number axis from the upper and lower sides of a complex plane, respectively.

Substitute (A6) for J_+ (A5). The interval from the function F^+ is calculated by closing the integration path over an infinite radius arc in the upper complex plane, which produces the result

$$J_+ = F(q^+)\exp(-\gamma R) - \int_{-\infty}^{\infty} \frac{dq'}{2\pi i}\left[\left(\frac{\exp[i(q'-q)R]}{q'-q-i\gamma} - \frac{\exp[-i(q'-q)R]}{q'-q+i\gamma}\right)F^-(q') + \frac{\exp[-i(q'-q)R]}{q'-q+i\gamma}F^-(q')\right].$$

The auxiliary function is added to and subtracted from the integrand to form a function of the type $(\sin x)/x$ (in parentheses) which is localized in an interval $q - q' < \pi/R$ (at $\gamma < \pi/R$). This enables us to take $F^-(q')$ out of the integration at a point $q' = q$. The remaining integral is readily calculated, as well as the integral with the last item, and we obtain the estimations

$$J_+ = [F(q^+) + F(q^-) - 2F^-(q)]\exp(-\gamma R)$$
$$= [2\pi i f(q) + F(q^+) - F^+(q) + F(q^-) - F^-(q)]\exp(-\gamma R)$$

or

$$J_+ \simeq 2\pi i f(q)\exp(-\gamma R). \tag{A7}$$

Similar transformations and approximations show that

$$J_- = F^+(q)\int_{-\infty}^{\infty}\frac{dq'}{2\pi i}\left(\frac{\exp[-i(q'-q)R]}{q'-q-i\gamma} - \frac{\exp[i(q'-q)R]}{q'-q+i\gamma}\right) + \int_{-\infty}^{\infty}\frac{dq'}{2\pi i}\frac{\exp[i(q'-q)R]}{q'-q+i\gamma}F^+(q').$$

In this case, both integrals are equal to zero; therefore

$$J_- \simeq 0. \tag{A8}$$

References

Aebi P, Erbudak M, Vanini F and Vvedensky D D 1992 *Surf. Sci. Lett.* **264** L181
Agostino R G, Amoddeo A, Catuki L S and Colavita E 1992 *Phys. Scr.* T **41** 149
Agostino R G, Küttel O M, Fasel R, Osterwalder J and Schlapbach L 1994 *Phys. Rev.* B **49** 13 820
Chiarello G, Formoso V, Caputi L S and Colavita E 1987 *Phys. Rev.* B **35** 5311
De Crescenzi M, Chainet E and Derrien J 1986 *Solid State Commun.* **57** 487
De Crescenzi M, Hitchcock A P and Tylisczak T 1989 *Phys. Rev.* B **39** 9839
Grebennikov V I and Sokolov O B 1992 *Phys. Scr.* T **41** 51
—— 1994 *Fiz. Metall. Metalloved.* **78** N5 113
Guy D E, Ruts Yu V, Sentemov C P, Grebennikov V I and Sokolov O B 1993 *Surf. Sci.* **298** 134
Guy D E, Ruts Yu V, Surnin D V, Grebennikov V I and Sokolov O B 1995 *Physica* B **208–209** 49
Sayers D E, Lytle F W and Stern E A 1970 *Adv. X-ray Anal.* **13** 29
Sinkovic B, Friedman D J and Fadley C S 1991 *J. Magn. Magn. Mater.* **92** 301
Woodruff D P 1987 *Surf. Sci.* **189–190** 64